Dalton Transactions

ROYAL SOCIETY OF CHEMISTRY

PAPER

View Article Online
View Journal | View Issue

Check for updates

Cite this: *Dalton Trans.*, 2021, **50**, 2654

Mechanism of nickel-catalyzed direct carbonyl-Heck coupling reaction: the crucial role of second-sphere interactions†

Jian-Hong Bian,[a] Wen-Yan Tong,[a] Chloe E. Pitsch,[b] Yan-Bo Wu *[a] and Xiaotai Wang *[c,b]

We present a detailed DFT mechanistic study on the first Ni-catalyzed direct carbonyl-Heck coupling of aryl triflates and aldehydes to afford ketones. The precatalyst $Ni(COD)_2$ is activated with the phosphine (phos) ligand, followed by coordination of the substrate PhOTf, to form [Ni(phos)(PhOTf)] for intramolecular PhOTf to Ni(0) oxidative addition. The ensuing phenyl-Ni(II) triflate complex substitutes benzaldehyde for triflate by an interchange mechanism, leaving the triflate anion in the second coordination sphere held by Coulomb attraction. The Ni(II) complex cation undergoes benzaldehyde C=O insertion into the Ni–Ph bond, followed by β-hydride elimination, to produce Ni(II)-bound benzophenone, which is released by interchange with triflate. The resulting neutral Ni(II) hydride complex leads to regeneration of the active catalyst following base-mediated deprotonation/reduction. The benzaldehyde C=O insertion is the rate-determining step. The triflate anion, while remaining in the second sphere, engages in electrostatic interactions with the first sphere, thereby stabilizing the intermediate/transition state and enabling the desired reactivity. This is the first time that such second-sphere interaction and its impact on cross-coupling reactivity has been elucidated. The new insights gained from this study can help better understand and improve Heck-type reactions.

Received 3rd December 2020,
Accepted 25th January 2021

DOI: 10.1039/d0dt04121a

rsc.li/dalton

Published on 29 January 2021. Downloaded by Shanxi University on 2/23/2021 11:59:06 PM.

Introduction

The transition metal-catalyzed Heck reaction, which cross couples alkenes with aryl halides/pseudohalides, has become one of the most important methods for constructing carbon–carbon bonds in chemical synthesis.[1] The general mechanism of the Heck reaction includes several key steps: (1) initial oxidative addition of the $C(sp^2)$–X bond to the metal, (2) migratory insertion of the alkene substrate into the metal–carbon bond, (3) β-hydride elimination to deliver the substituted alkene product, and (4) base-mediated reductive elimination to regenerate the catalyst.[2] A carbonyl version of the Heck reaction replaces the alkene with an aldehyde substrate, which undergoes carbonyl (C=O) migratory insertion to afford a ketone product.[3] Ketones are an important class of organic compounds, and the ketone functionality engages in many reactions to give alkanes, alkenes, alcohols, esters, *etc*.

The Newman group has recently made a breakthrough in the emerging area of carbonyl-Heck reactions by developing a Ni-catalyzed direct coupling of aryl triflates with aryl aldehydes to form ketones,[4] as shown by the representative reaction in Scheme 1. This method shows remarkable simplicity, generality, and efficiency in stark contrast to the earlier protocols that required stoichiometric conversion of aldehydes to imines[5]/hydrazones[6]/enamines[7] or photoredox catalysis to generate acyl radicals.[8] Furthermore, the catalyst system is based on a

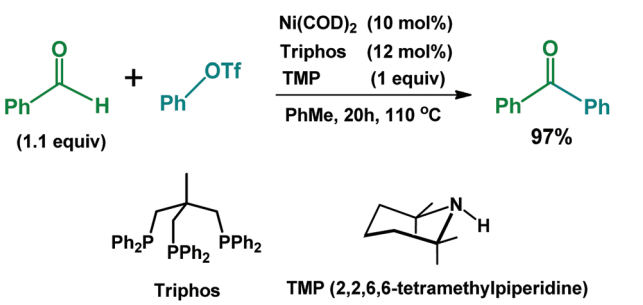

Scheme 1 Ni-catalyzed direct carbonyl-Heck coupling.

[a]*Key Laboratory of Materials for Energy Conversion and Storage of Shanxi Province and Institute of Molecular Science, Shanxi University, Taiyuan 030006, P. R. China. E-mail: wyb@sxu.edu.cn*
[b]*Department of Chemistry, University of Colorado Denver, Campus Box 194, P. O. Box 173364, Denver, Colorado 80217-3364, USA. E-mail: xiaotai.wang@ucdenver.edu*
[c]*Hoffmann Institute of Advanced Materials, Shenzhen Polytechnic, 7098 Liuxian Boulevard, Nanshan District, Shenzhen 518055, P. R. China*

†Electronic supplementary information (ESI) available. See DOI: 10.1039/d0dt04121a

This journal is © The Royal Society of Chemistry 2021

Published on 29 January 2021. Downloaded by Shanxi University on 2/23/2021 11:59:06 PM.

common, commercially available nickel reagent, $Ni(COD)_2$, and as such, the work exemplifies successful utilization of earth-abundant 3d transition metal catalysts to realize important organic transformations. There has been ongoing intense interest in developing such base metal catalysts because they are not only more sustainable, but can also effect new modes of reactivity.[1g,9] On yet another note, the phosphine ligand Triphos and the amine base TMP were both used for the first time as effective additives for Ni-catalyzed cross-coupling reactions.[4]

Newman *et al.* tested their catalyst system on traditional Heck reactions of organotriflates with styrene/butyl vinyl ether, and obtained the Heck products as expected. They also studied the kinetic isotope effect and observed a moderate, likely secondary KIE of 1.3, which suggested no C–H cleavage in the rate-determining step.[4] Thus, this novel carbonyl-Heck reaction is assumed to proceed through the general catalytic cycle for Heck reactions, but its detailed mechanism is unclear and warrants exploration. An intriguing observation of the reaction is that aryl triflates rather than aryl halides must be used to provide the desired reactivity.

There are a number of computational studies on nickel-catalyzed traditional Heck reactions.[10] In this DFT computational study, we examine all the important phases of the carbonyl-Heck reaction and propose a detailed mechanism. The highlight of the mechanism is the elucidation of crucial second-sphere interactions in an unprecedented ion-pair pathway for the migratory insertion and β-hydride elimination. We discuss our findings in context, with a goal of gaining new and useful insights into Heck-type cross-coupling reactions.

Computational methods

The reaction shown in Scheme 1 was computed using the full molecule of every reagent without any truncation or symmetry constraint. Geometries were optimized and characterized by frequency calculations to be energy minima (zero imaginary frequencies) or transition states (only one imaginary frequency) at the B3LYP[11]/BS1 level in the gas phase, BS1 designating a mixed basis set of SDD[12] for nickel and iodine and 6-31G(d) for other atoms. The energies were then refined by M06[13]/BS2//B3LYP/BS1 single-point energy calculations in toluene (the reaction solvent) with the SMD[14] solvation model, BS2 denoting a mixed basis set of SDD for nickel and iodine and 6-311++G(d,p) for other atoms. The refined energies were converted to zero-point energy-corrected free energies at 298.15 K and 1 atm, using the B3LYP/BS1 harmonic frequencies. This combined B3LYP/M06 method has been successfully used to study many transition metal-catalyzed reactions,[15–32] including organonickel systems.[28–32] For benchmarking purposes, the key transition states and intermediates were subject to reoptimization with M06/BS1 and single-point energy calculation with M06/BS2//M06/BS1, and the M06/BS2//M06/BS1 outcomes were consistent with the M06/BS2//B3LYP/BS1 results (Fig. S1†). In addition, the key transition states and intermediates were subject to reoptimization with the solvent correction included using the SMD model, and the outcomes were consistent with the results obtained with optimization in vacuum/the gas phase (Fig. S2†). Natural charges were obtained for selected structures by natural population analysis (NPA) at the M06/BS2 level in toluene using the SMD solvation model. All calculations were performed with Gaussian 09.[33]

Results and discussion

Initiation and oxidative addition

The precatalyst $Ni(COD)_2$ (**1**) is activated by reacting with Triphos in an approximately 1 : 1 mole ratio, for which we have considered various possible products (Fig. S3†). The three-coordinate complex **2** is the most stable species generated, with Triphos acting as a bidentate chelator,[34] as shown in Fig. 1. This initial process has a sizable driving force (ΔG = −14.0 kcal mol^{-1}). Replacement of COD in **2** with phenyl triflate (PhOTf) would deliver the substrate to the Ni(0) center, for which we have found the most stable complex **3** wherein Ni(0) binds PhOTf *via* η^2–π coordination.

The geometry of **3** is such that it brings the Ni(0) center and the Ph–OTf bond into a proper spatial relationship. This symphoria[35] facilitates the intramolecular Ph–OTf to Ni(0) two-electron oxidative addition *via* the three-center transition state **TS1** with a small overall activation energy ($\Delta G^{\ddagger}$ = 13.5 kcal mol^{-1} with respect to **2**). **TS1** proceeds to the stable square planar Ni(II) d^8 complex **4**, and the oxidative addition process is irreversible (ΔG = −22.0 kcal mol^{-1}). We have also considered and ruled out the single electron transfer (SET) pathway for the oxidative addition (Fig. S4†).

Benzaldehyde insertion into Nickel–phenyl bond

We have considered the associative, dissociative, and interchange pathways for intermediate **4** to uptake the substrate benzaldehyde for its C=O insertion into the Ni–Ph bond. The associative pathway was ruled out because no five-coordinate

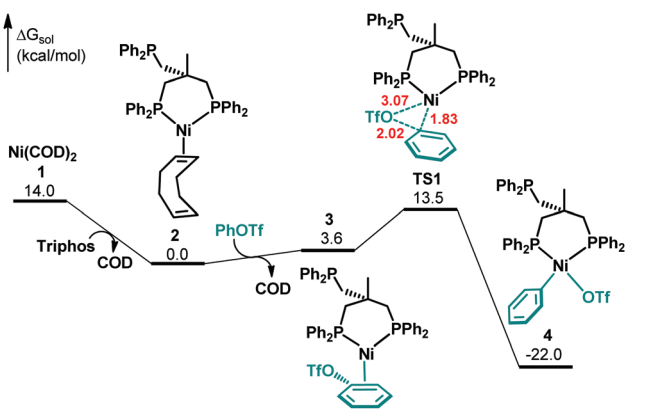

Fig. 1 Free energy profile for the precatalyst initiation followed by PhOTf oxidative addition. Selected bond distances in red font are given in Å (the same below).

Published on 29 January 2021. Downloaded by Shanxi University on 2/23/2021 11:59:06 PM.

benzaldehyde-bearing complexes/transition states could be found directly from **4**. Apart from possible orbital effects,[36] the steric hindrance of the ligand set in **4** could block the associative pathway.

Theoretical studies of Pd/Ni-catalyzed Heck reactions have invoked a cationic pathway in which the alkene substrate binds to a three-coordinate cationic species derived from dissociation of an anion ligand.[10a,37] This prior knowledge led us to consider dissociation of the triflate anion from **4**, which yields the three-coordinate cationic complex **5** with a 32.0 kcal mol^{-1} free energy increase (Fig. 2). Coordination of benzaldehyde to **5** through a weak Ni–O(carbonyl) dative bond is only slightly exergonic, and the resulting complex **6** lies higher than **4** by 24.2 kcal mol^{-1}. Complex **6** could launch the benzaldehyde C=O insertion into the Ni–Ph bond *via* the four-center transition state **TS2**. The insertion step alone *via* **TS2** would be viable with an activation energy of 17.4 kcal mol^{-1}, but **TS2** is 41.6 kcal mol^{-1} with respect to **4** (the preceding lowest point), and this energy span[38] is too large to be reasonable for the reaction. Thus, the dissociative pathway through **TS2** would be disfavored. The key factor is the large energy cost incurred by the triflate anion dissociating from **4** and separating from the complex cation **5**, which cannot be compensated for by forming a weak Ni–O(carbonyl) dative bond in **6**. In comparison, a previous study on Ni-catalyzed Heck reactions found a slightly exergonic dissociative substitution of alkene for triflate (ΔG = −1.8 kcal mol^{-1}) for a Ni(II) complex,[10a] which could be due to a robust Ni/C=C coordination having synergistic σ donation and π backbonding.

We have also considered the loss of the P coordination *cis* to the phenyl in **4** to accommodate benzaldehyde insertion (see the blue path in Fig. 2). That dissociation is uphill by 38.2 kcal mol^{-1} because it disrupts the six-membered chelate ring in **4**. The succeeding benzaldehyde C=O insertion barrier **TS3** is 41.2 kcal mol^{-1} relative to **4**, which rules out this dissociative pathway. In contrast, it has been proposed that in Heck reactions, monodentate phosphine ligands can dissociate from Pd/Ni intermediates to vacate a coordination site for an incoming alkene.[10b,37a,39]

Having excluded the associative and dissociative pathways as disfavored, we have traced the favored interchange pathway, as shown in Fig. 3. The entering benzaldehyde exchanges with the leaving triflate *via* **TS4**, which is a low barrier (8.3 kcal mol^{-1} with respect to **4**) and proceeds to the ion pair **11**. It is worth noting that no such interchange pathway has previously been computed for alkene uptake in Pd/Ni-catalyzed Heck reactions. The most salient feature of **11** is that the triflate anion remains in the second coordination sphere through Coulomb attractive interactions with the first sphere, showing a nickel–triflate ionic bond at 3.53 Å. This is crucial because separation of the triflate anion from the first sphere would incur a large energy cost and hence shut down the reaction, as discussed above (see Fig. 2). Intermediate **11** undertakes C=O insertion into the Ni–Ph bond within the first coordination sphere while retaining the triflate in the second sphere, thus transforming into **TS5**. This energy barrier is 25.7 kcal mol^{-1} with respect to **4**, which can be overcome at the reaction temperature (110 °C). **TS5** proceeds to the ion pair **12**, completing the C–C coupling and forming a cationic nickel(II) alkoxide complex for the subsequent β-hydride elimination and ketone production.

On another note, we have considered and ruled out the aldehyde C–H activation pathway through **11**, which would have a much higher activation energy barrier (Fig. S5†).

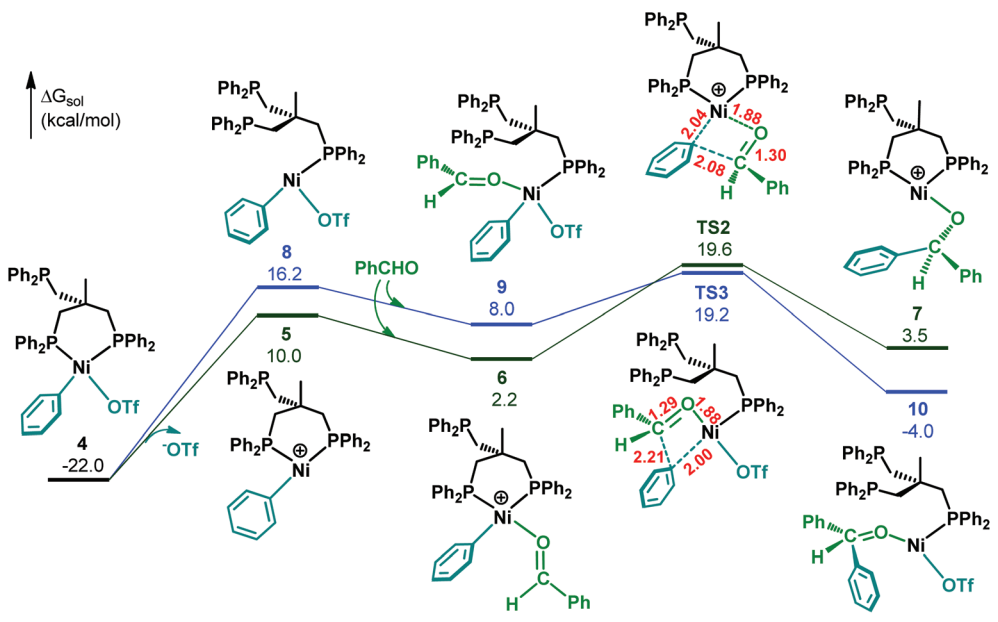

Fig. 2 Free energy profile for the dissociative pathways of benzaldehyde ligation and insertion.

 This journal is © The Royal Society of Chemistry 2021

Published on 29 January 2021. Downloaded by Shanxi University on 2/23/2021 11:59:06 PM.

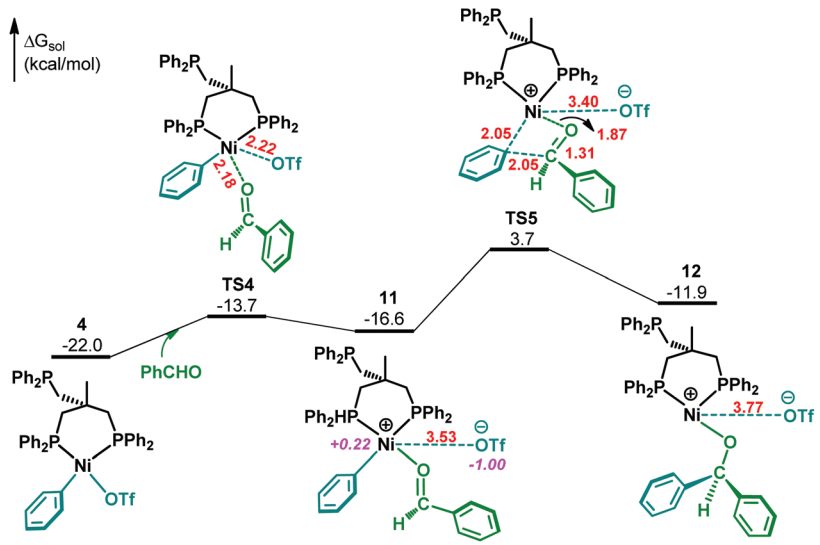

Fig. 3 Free energy profile for the interchange pathway of benzaldehyde ligation and insertion. Natural charges in |e| on selected atoms in **11** are shown in italic purple font.

β-Hydride elimination and ketone production

As shown in Fig. 4, the nickel(II) alkoxide complex cation in **12** cannot undertake β-hydride elimination directly because of the large Ni···$H_β$ span. Intra-alkoxide rotation around the C–O single bond affords the isomer **13**, which brings the Ni(II) and $H_β$ atoms into proximity. There are significant agostic interactions in **13**, as revealed by the Ni···$H_β$ contact at 1.70 Å and the lengthened C–H bond at 1.23 Å. These interactions evidently facilitate the β-hydride elimination *via* **TS6** to give the ion pair **14**, which has a square planar Ni(II) complex cation bearing benzophenone and interacting with the triflate in the second sphere. The product benzophenone is released through the interchange transition state **TS7** where the triflate moves into the first sphere to replace benzophenone forming the neutral nickel(II) hydride complex **15**. The barriers **TS6** and **TS7** are each considerably lower than the C=O insertion barrier **TS5** shown in Fig. 3. The reaction coordinate continues being thermodynamically downhill beyond oxidative addition, with an overall driving force of 3.3 kcal mol^{-1} from **4** through **15** (Fig. 3 and 4).

Base-induced reduction and catalyst regeneration

As shown in Fig. 5, the amine base TMP attacks the hydrido-Ni(II) complex **15** *via* **TS8** ($ΔG^‡$ = 16.5 kcal mol^{-1}), using both the

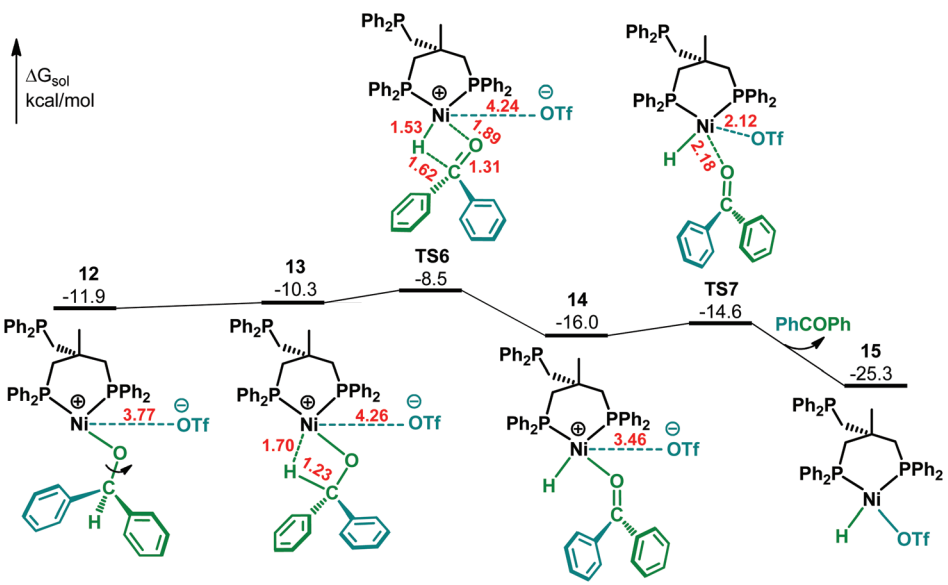

Fig. 4 Free energy profile for the β-hydride elimination and ketone product release.

Published on 29 January 2021. Downloaded by Shanxi University on 2/23/2021 11:59:06 PM.

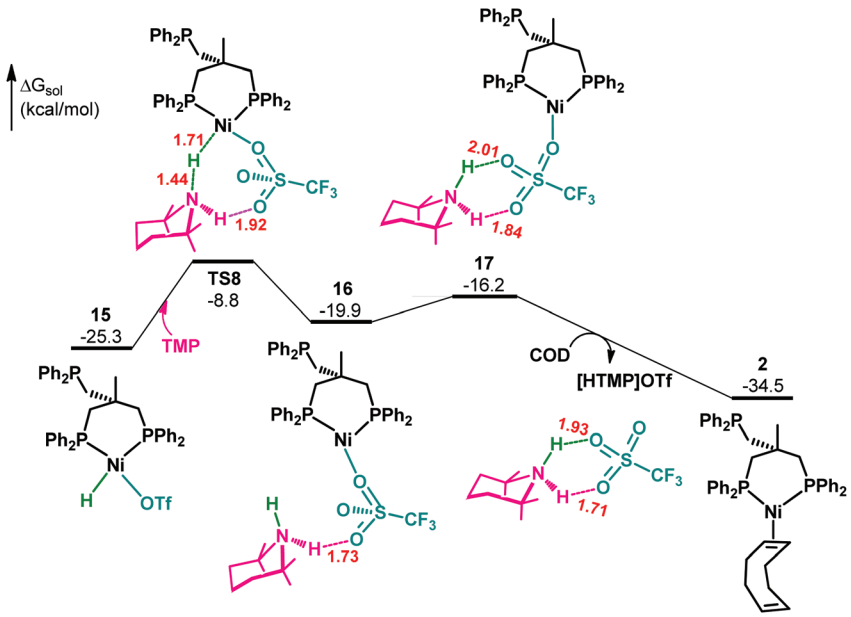

Fig. 5 Free energy profile for the base-induced reduction and catalyst regeneration.

nitrogen lone pair and the nitrogen-bound hydrogen, the former interacting with the Ni(II)-bound hydrogen and the latter forming a hydrogen bond with one triflate oxygen atom. The hydrogen bonding interaction helps lower the energy of **TS8**. In **TS8**, the Ni(II)-bound hydrogen is transitioning from hydridic to protonic, leaving two electrons to the Ni(II) center. This leads to a proton transfer and formal two-electron reduction which yields the Ni(0) complex **16** bearing a neutral hydrogen-bonded ion pair [HTMP]OTf. Complex **16** isomerizes to **17** with a doubly hydrogen-bonded ion pair [HTMP]OTf, which then substitutes COD for [HTMP]OTf to regenerate the active species **2**. It is this highly exergonic substitution (ΔG = −18.3 kcal mol^{-1}) that drives the reaction from **15** through the regeneration of **2** (ΔG = −9.2 kcal mol^{-1}).

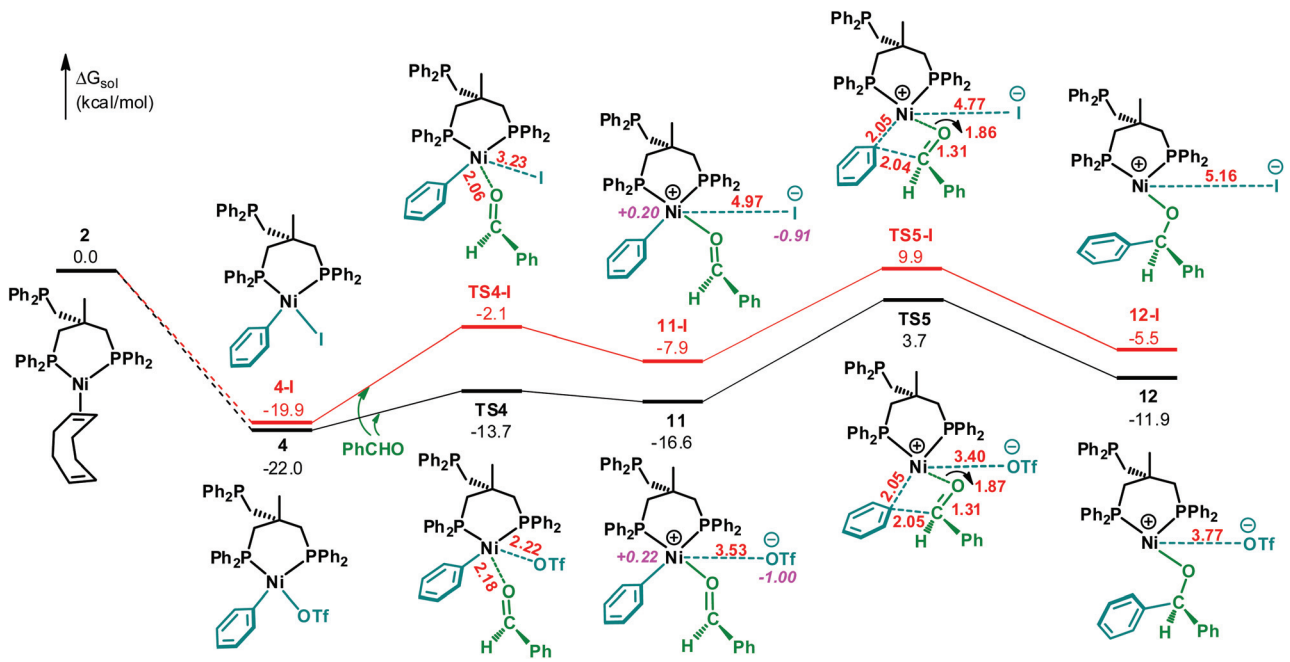

Fig. 6 Comparing the pathways of benzaldehyde ligation and insertion involving two different substrates: PhI, the red path; PhOTf, the black path (shown earlier in Fig. 3). Natural charges in |e| on selected atoms in **11** and **11-I** are shown in italic purple font. The hyphenated letter I in a name designates a species in the reaction involving PhI.

 This journal is © The Royal Society of Chemistry 2021

Published on 29 January 2021. Downloaded by Shanxi University on 2/23/2021 11:59:06 PM.

The complete reaction coordinate has now been mapped out, with every intermediate and transition state molecularly well defined and energetically reasonable (Fig. 1 and 3–5). The overall sequence of reaction—from the generation of **2** through the regeneration of **2**—is highly favorable thermodynamically (ΔG = –34.5 kcal mol^{-1}). The largest energy span is from **4** to **TS5**, 25.7 kcal mol^{-1} (Fig. 3), and the benzaldehyde C=O insertion into the Ni–Ph bond *via* **TS5** is the rate-determining step. In summary, the computations support the experimentalists' assumption of the Heck reaction-like mechanism and their observation of no C–H cleavage in the rate-determining step.

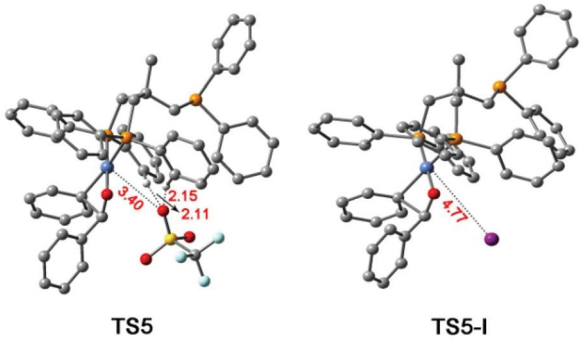

Fig. 7 Optimized structures of **TS5** and **TS5-I** in ball-and-stick models, with hydrogen atoms omitted for clarity except those engaging in C–H···O hydrogen bonds.

Comparing phenyl iodide and phenyl triflate as substrates

When phenyl halides instead of phenyl triflate are employed as substrates, the yield for the title reaction is low (<10%).[4] To explain this experimental observation, we have studied the mechanism of the reaction involving phenyl iodide and found it analogous to the reaction with phenyl triflate (Fig. S6–S9†). The important part of the mechanism, which contains the rate-determining benzaldehyde insertion step, is presented here in comparison with its triflate counterpart (Fig. 6).

The two oxidative addition products, **4** and **4-I**, are of similar energy relative to the common precursor **2**. As **4** and **4-I** undertake ligand interchange with benzaldehyde, the reaction favors the former over the latter in both kinetics and thermodynamics. The resulting ion pairs **11** and **11-I** share the same complex cation but have different anions, and their cation–-

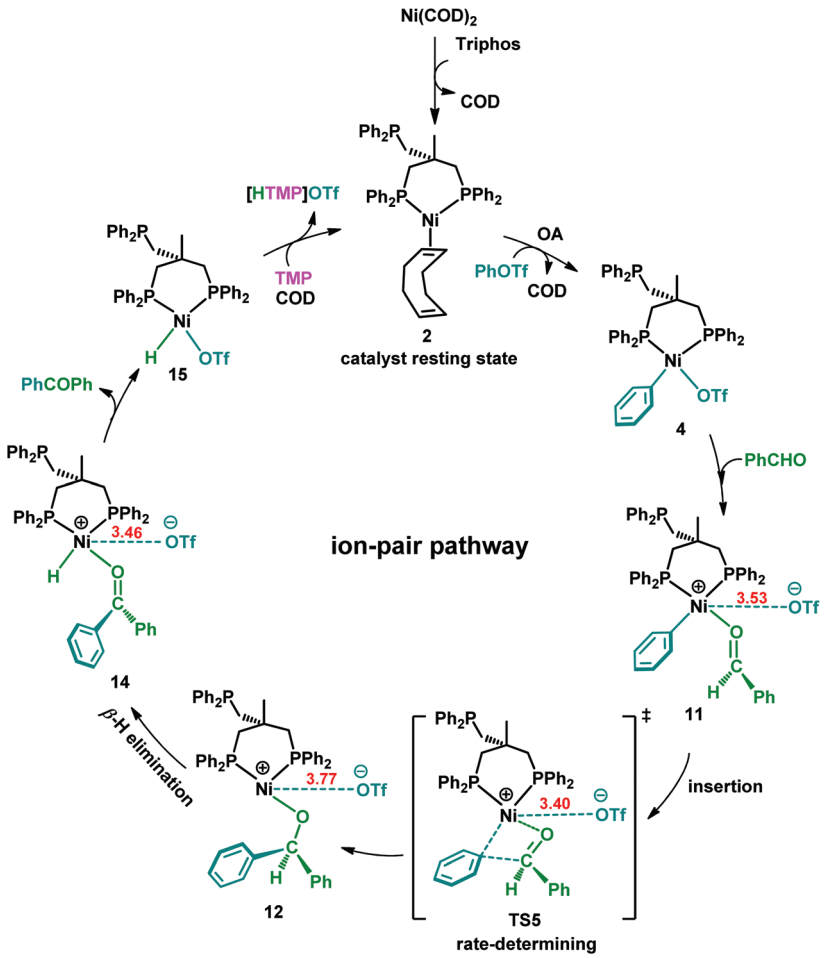

Scheme 2 Summary of the mechanism for Ni-catalyzed carbonyl-Heck coupling.

Published on 29 January 2021. Downloaded by Shanxi University on 2/23/2021 11:59:06 PM.

anion distances differ significantly (3.53 *vs.* 4.97 Å). Intermediates **11** and **11-I** transform to the corresponding **TS5** and **TS5-I**, the benzaldehyde-inserting and rate-limiting transition states. Fig. 7 shows the optimized geometries of **TS5** and **TS5-I**, which we have examined closely to identify the structural factors affecting their relative energies. The difference in cation–anion distance persists in **TS5** and **TS5-I** (3.40 *vs.* 4.77 Å), indicating stronger Coulomb attraction in **TS5**. In addition, **TS5** contains two second-sphere C–H(ligand)···O(triflate) hydrogen bonds with H···O distances at 2.11 and 2.15 Å, which is a stabilizing factor. These second-sphere interactions set **TS5** and **TS5-I** apart energetically. **TS5** is 25.7 kcal mol^{-1} with respect to **4**, whereas **TS5-I** is 29.8 kcal mol^{-1} with respect to **4-I**. Thus, the overall activation energy of the reaction with phenyl iodide is 4.1 kcal mol^{-1} higher than that of the reaction with phenyl triflate. This gap clearly explains the much lower yield of the reaction that used phenyl iodide as a substrate.

We have also considered the dissociation of OTf^-/I^- from **11**/**11-I** in Fig. 6 and computed the two alternative parallel pathways. These would be of much higher energy and hence disfavored, and the difference in rate favoring PhOTf over PhI would be even larger (Fig. S10†).

Limitations of this DFT study

There are mainly two experimental features that this DFT study cannot fully explain. First, when other base additives, such as PMP (pentamethylpiperidine) and i-Pr_2NEt (*N,N*-diisopropylethylamine), were used in place of TMP, the yields would decrease from 97% to 87% and 20%. We have computed the PMP-associated energy profile whose deprotonation barrier **TS11** is higher due to the greater steric hindrance of PMP and the absence of PMP–OTf hydrogen bonding (Fig. S11†). Thus, the difference in energy between **TS11** and **15**, 26.8 kcal mol^{-1}, becomes the largest energy span of the entire pathway. This energy barrier is somewhat greater than 25.7 kcal mol^{-1}, the energy span of the pathway involving TMP, thereby explaining the lower yield of 87% obtained with PMP. Nevertheless, DFT calculations could not explain why i-Pr_2NEt gave a very low yield of 20% (Fig. S12†); it might have a side reaction with the catalyst, thus reducing its activity.

Second, while Triphos gave good yields for both simple and complex aldehyde substrates, a diphos ligand like dppp [1,3-bis(diphenylphosphino)propane] only worked well for simple aldehydes such as PhCHO (Fig. S13–S16†). As a partial explanation, the computations show that the square planar Ni(II) intermediate **4** bearing Triphos in bidentate mode is more stable towards isomerization to the inactive tetrahedral complex, as compared with the square planar Ni(II) intermediate bearing dppp (Fig. S17†).

Conclusions

We have established by DFT computation a detailed and plausible mechanism for the title reaction. The key points of the mechanism are summarized in Scheme 2. The ligand Triphos turns the precatalyst $Ni(COD)_2$ over into the active species **2**, which starts the catalytic cycle by taking up PhOTf for facile intramolecular PhOTf to Ni(0) oxidative addition to form the square planar Ni(II) phenyl triflate complex **4**. This complex substitutes benzaldehyde for triflate by an interchange mechanism to give the ion pair **11** with the triflate anion held in the second sphere by electrostatic attractive forces. The Ni(II) complex cation in **11** undertakes benzaldehyde insertion into the Ni–Ph bond *via* **TS5**, the rate-determining energy barrier. The resulting Ni(II) alkoxide complex **12** undergoes β-hydride elimination to form the product benzophenone, which is released from complex **14** by interchange with triflate. The neutral hydrido-Ni(II) complex **15** is subject to base (TMP)-mediated deprotonation/reduction, followed by COD coordination, to regenerate **2**.

The triflate anion remains in the second sphere and interacts with the first sphere throughout the C=O insertion and β-hydride elimination processes, and these constitute an ion-pair pathway that has not been proposed and elucidated by previous mechanistic studies of Heck-type reactions. The second-sphere interactions help lower the energy of the intermediate/transition state, thereby enabling the desired reactivity. By comparison, the halide anion (*e.g.*, iodide) interacts with the first sphere much less strongly, which results in considerably higher energy barriers and lower product yields for the reactions involving phenyl halide substrates. To our knowledge, this is the first time that such second-sphere interaction and its impact on cross-coupling reactivity has been elucidated.

This DFT computational study reveals how the common nickel reagent $Ni(COD)_2$, in tandem with the ligand and base additives, promotes the Ni-catalyzed direct carbonyl-Heck coupling of aryl triflates with aryl aldehydes to form ketones. The new mechanistic insights gained from this study are expected to have implications for Heck-type cross-coupling reactions.

Conflicts of interest

There are no conflicts to declare.

Acknowledgements

We acknowledge support for this work from the NSFC (Grant No. 21720102006, 21273140, and 21471092), the Natural Science Foundation of Shanxi Province (Grant No. 201901D111018 and 201901D111014), the One Hundred-Talent Program of Shanxi Province, the OIT Program, the Shanxi "1331 Project" Engineering Research Center (PT201807), the Shanxi 1331KIRT, the HPC of Shanxi University, the Hoffmann Institute of Advanced Materials of Shenzhen Polytechnic, and the University of Colorado Denver. We thank Dr Jiandong Guo for his help with computing a transition state structure.

 This journal is © The Royal Society of Chemistry 2021

Published on 29 January 2021. Downloaded by Shanxi University on 2/23/2021 11:59:06 PM.

Notes and references

1 (*a*) R. F. Heck, *J. Am. Chem. Soc.*, 1969, **91**, 6707–6714; (*b*) R. F. Heck and J. P. Nolley, *J. Org. Chem.*, 1972, **37**, 2320–2322; (*c*) A. De Meijere and F. E. Meyer, *Angew. Chem., Int. Ed.*, 1994, **33**, 2379–2411; (*d*) I. P. Beletskaya and A. V. Cheprakov, *Chem. Rev.*, 2000, **100**, 3009–3066; (*e*) A. B. Dounay and L. E. Overman, *Chem. Rev.*, 2003, **103**, 2945–2964; (*f*) D. Mc Cartney and P. J. Guiry, *Chem. Soc. Rev.*, 2011, **40**, 5122–5150; (*g*) J. M. Weber, A. R. Longstreet and T. F. Jamison, *Organometallics*, 2018, **37**, 2716–2722.

2 (*a*) L. Xue and Z. Lin, *Chem. Soc. Rev.*, 2010, **39**, 1692–1705; (*b*) J. P. Knowles and A. Whiting, *Org. Biomol. Chem.*, 2007, **5**, 31–44; (*c*) P. Surawatanawong, Y. Fan and M. B. Hall, *J. Organomet. Chem.*, 2008, **693**, 1552–1563; (*d*) P. Fristrup, S. Le Quement, D. Tanner and P.-O. Norrby, *Organometallics*, 2004, **23**, 6160–6165; (*e*) M. Ahlquist, P. Fristrup, D. Tanner and P.-O. Norrby, *Organometallics*, 2006, **25**, 2066–2073.

3 J. Ruan and J. Xiao, *Acc. Chem. Res.*, 2011, **44**, 614–626.

4 J. K. Vandavasi, X. Hua, H. B. Halima and S. G. Newman, *Angew. Chem., Int. Ed.*, 2017, **56**, 15441–15445.

5 T. Ishiyama and J. Hartwig, *J. Am. Chem. Soc.*, 2000, **122**, 12043–12044.

6 A. Takemiya and J. F. Hartwig, *J. Am. Chem. Soc.*, 2006, **128**, 14800–14801.

7 (*a*) J. Ruan, O. Saidi, J. A. Iggo and J. Xiao, *J. Am. Chem. Soc.*, 2008, **130**, 10510–10511; (*b*) P. Colbon, J. Ruan, M. Purdie and J. Xiao, *Org. Lett.*, 2010, **12**, 3670–3673.

8 X. Zhang and D. W. C. MacMillan, *J. Am. Chem. Soc.*, 2017, **139**, 11353–11356.

9 (*a*) B. Su, Z.-C. Cao and Z.-J. Shi, *Acc. Chem. Res.*, 2015, **48**, 886–896; (*b*) Y.-Y. Li, S.-L. Yu, W.-Y. Shen and J.-X. Gao, *Acc. Chem. Res.*, 2015, **48**, 2587–2598; (*c*) V. Rodriguez-Ruiz, R. Carlino, S. Bezzenine-Lafollee, R. Gil, D. Prim, E. Schulz and J. Hannedouche, *Dalton Trans.*, 2015, **44**, 12029–12059.

10 (*a*) T. M. Gogsig, J. Kleimark, S. O. Lill, S. Korsager, A. T. Lindhardt, P. O. Norrby and T. Skrydstrup, *J. Am. Chem. Soc.*, 2012, **134**, 443–452; (*b*) B.-L. Lin, L. Liu, Y. Fu, S.-W. Luo, Q. Chen and Q.-X. Guo, *Organometallics*, 2004, **23**, 2114–2123; (*c*) V. H. M. da Silva, A. A. C. Braga and T. R. Cundari, *Organometallics*, 2016, **35**, 3170–3181.

11 (*a*) C. Lee, W. Yang and R. G. Parr, *Phys. Rev. B: Condens. Matter Mater. Phys.*, 1988, **37**, 785–789; (*b*) A. D. Becke, *J. Chem. Phys.*, 1993, **98**, 1372–1377; (*c*) A. D. Becke, *J. Chem. Phys.*, 1993, **98**, 5648–5652; (*d*) P. J. Stephens, F. Devlin, C. Chabalowski and M. J. Frisch, *J. Phys. Chem.*, 1994, **98**, 11623–11627.

12 (*a*) D. Andrae, U. Haussermann, M. Dolg, H. Stoll and H. Preuss, *Theor. Chim. Acta*, 1990, **77**, 123–141; (*b*) M. Dolg, U. Wedig, H. Stoll and H. Preuss, *J. Chem. Phys.*, 1987, **86**, 866–872.

13 Y. Zhao and D. G. Truhlar, *Theor. Chem. Acc.*, 2008, **120**, 215–241.

14 A. V. Marenich, C. J. Cramer and D. G. Truhlar, *J. Phys. Chem. B*, 2009, **113**, 6378–6396.

15 Y.-F. Yang, X. Hong, J.-Q. Yu and K. N. Houk, *Acc. Chem. Res.*, 2017, **50**, 2853–2860.

16 V. Palani, C. L. Hugelshofer, I. Kevlishvili, P. Liu and R. Sarpong, *J. Am. Chem. Soc.*, 2019, **141**, 2652–2660.

17 Z. Dong, G. Lu, J. Wang, P. Liu and G. Dong, *J. Am. Chem. Soc.*, 2018, **140**, 8551–8562.

18 Y. Dang, S. Qu, Z.-X. Wang and X. Wane, *J. Am. Chem. Soc.*, 2014, **136**, 986–998.

19 H. Shao, Y. Wang, C. W. Bielawski and P. Liu, *ACS Catal.*, 2020, **10**, 3820–3827.

20 J. Wu, X. Li, X. Qi, X. Duan, W. L. Cracraft, I. A. Guzei, P. Liu and W. Tang, *J. Am. Chem. Soc.*, 2019, **141**, 19902–19910.

21 Y. Dang, S. Qu, Y. Tao, X. Deng and Z.-X. Wang, *J. Am. Chem. Soc.*, 2015, **137**, 6279–6291.

22 T.-T. Liu, S.-Y. Tang, B. Hu, P. Liu, S. Bi and Y.-Y. Jiang, *J. Org. Chem.*, 2020, **85**, 12444–12455.

23 J.-L. Yu, S.-Q. Zhang and X. Hong, *J. Am. Chem. Soc.*, 2017, **139**, 7224–7243.

24 J. S. Cannon, L. Zou, P. Liu, Y. Lan, D. J. O'Leary, K. N. Houk and R. H. Grubbs, *J. Am. Chem. Soc.*, 2014, **136**, 6733–6743.

25 A. Bartoszewicz, G. G. Miera, R. Marcos, P.-O. Norrby and B. Martin-Matute, *ACS Catal.*, 2015, **5**, 3704–3716.

26 Y. Ye, I. Kevlishvili, S. Feng, P. Liu and S. L. Buchwald, *J. Am. Chem. Soc.*, 2020, **142**, 10550–10556.

27 Y. Yang and P. Liu, *ACS Catal.*, 2015, **5**, 2944–2951.

28 X. Ren, Y. Lu, G. Lu and Z.-X. Wang, *Org. Lett.*, 2020, **22**, 2454–2459.

29 C. Zhang, R. Zhao, W. M. Dagnaw, Z. Liu, Y. Lu and Z.-X. Wang, *J. Org. Chem.*, 2019, **84**, 13983–13991.

30 P.-P. Chen, H. Zhang, B. Cheng, X. Chen, F. Cheng, S.-Q. Zhang, Z. Lu, F. Meng and X. Hong, *ACS Catal.*, 2019, **9**, 9589–9598.

31 S.-Q. Zhang, B. L. H. Taylor, C.-L. Ji, Y. Gao, M. R. Harris, L. E. Hanna, E. R. Jarvo, K. N. Houk and X. Hong, *J. Am. Chem. Soc.*, 2017, **139**, 12994–13005.

32 L. Hie, N. F. F. Nathel, T. K. Shah, E. L. Baker, X. Hong, Y.-F. Yang, P. Liu, K. N. Houk and N. K. Garg, *Nature*, 2015, **524**, 79–83.

33 M. J. Frisch, *et al.*, *Gaussian 09 Revision D.01*, Gaussian Inc., Wallingford, CT, 2013.

34 (*a*) M. Kandiah, G. S. McGrady, A. Decken and P. Sirsch, *Inorg. Chem.*, 2005, **44**, 8650–8652; (*b*) A. Petuker, S. Mebs, N. Schuth, P. Gerschel, M. L. Reback, B. Mallick, M. van Gastel, M. Haumann and U.-P. Apfel, *Dalton Trans.*, 2017, **46**, 907–917.

35 R. T. Morrison and R. N. Boyd, *Organic Chemistry*, 1992, 6th edn, Prentice Hall, New Jersey, pp. 1032.

36 D. L. Thorn and R. Hoffmann, *J. Am. Chem. Soc.*, 1978, **100**, 2079–2090.

37 (*a*) C. Bäcktorp and P.-O. Norrby, *Dalton Trans.*, 2011, **40**, 11308–11314; (*b*) S. T. Henriksen, P.-O. Norrby, P. Kaukoranta and P. G. Andersson, *J. Am. Chem. Soc.*,

2008, **130**, 10414–10421; (*c*) S. J. Sabounchei, M. Hosseinzadeh, S. Salehzadeh, F. Maleki and R. W. Gable, *Inorg. Chem. Front.*, 2017, **4**, 2107–2118.

38 (*a*) S. Kozuch and S. Shaik, *J. Am. Chem. Soc.*, 2006, **128**, 3355–3365; (*b*) S. Kozuch and S. Shaik, *Acc. Chem. Res.*, 2011, **44**, 101–110.

39 (*a*) M.-T. Lee, H. M. Lee and C.-H. Hu, *Organometallics*, 2007, **26**, 1317–1324; (*b*) S. Y. Tang, Q. X. Guo and Y. Fu, *Chem. – Eur. J.*, 2011, **17**, 13866–13876; (*c*) K. Geoghegan, P. Evans, I. Rozas and I. Alkorta, *Chem. – Eur. J.*, 2012, **18**, 13379–13387; (*d*) L. Liu, Y. Liu, B. Ling and S. Bi, *J. Organomet. Chem.*, 2017, **827**, 56–66.

Published on 29 January 2021. Downloaded by Shanxi University on 2/23/2021 11:59:06 PM.

This journal is © The Royal Society of Chemistry 2021